NJC

Check for updates

Characterization of aggregated morphologies derived from mono- and bis-arylbenzamides – potential alpha-helix mimetics†

Oleg V. Kulikov, [iD] *[a] Yulia V. Sevryugina,[b] Arshad Mehmood[b] and Ishu Saraogi[c]

We report here the synthesis and self-assembly studies of a family of benzamide backbone oligomers bearing various alkyl side chains (*e.g.*, isopropyl, isobutyl, and 2-ethylpentyl), which are potential alpha-helix mimetics capable of disrupting protein–protein interactions. Electron microscopy data (*i.e.*, SEM and TEM concentration series) are indicative of the formation of various aggregates, such as micro- and nanofibers, and spherical beads, which are dominated by bis-oligoamide structures and may have resulted from intermolecular H-bonding, π–π stacking, and amide group dipole electrostatic attraction as evidenced by single crystal X-ray analysis. Thus, the aggregation behaviour was shown to depend on the number of repeat units in the oligoamide scaffold featuring elongated aggregates for bis-tetramers, whereas bis-dimers tend to form microspheres in a wide range of concentrations examined. We hypothesize that higher oligomers possessing an extended arylamide backbone are prone to efficiently crystallize with one another by interdigitation of their alkyl side chains leading predominantly to rod-like morphologies and fibrous crystals. The structural findings presented here can be potentially used in the rational design of supramolecular architectures based on arylamide peptidomimetics.

Introduction

Over the years, there has been intense interest in developing non-peptidic small-molecule alpha-helix mimetics[1] due to their potential ability to disrupt protein–protein interactions (PPIs). Different synthetic platforms[2–6] (*e.g.*, indanes, terphenyls, pyridyl-pyridones, pyridazines, polycyclic ethers, *etc.*) have been reported to efficiently inhibit alpha-helix mediated PPIs. A contribution from the Hamilton lab[3–6,7a,b] has extended the principles of molecular design and developed synthetic strategies for small-molecule inhibitors of therapeutically relevant protein targets important in cancer and infectious diseases, Alzheimer's disease, type II diabetes, HIV, *etc.* Importantly, the formation of colloidal aggregates from small drug molecules may inhibit enzymes and other proteins as was reported by the Shoichet group.[7c,d] This interesting phenomenon should not be underestimated when assessing the structure–activity relationship (SAR) of promiscuous

drugs since it may cause false-positive inhibition through the self-association of organic molecules in aqueous solutions.

Herein, we report the synthesis and self-assembly in the solid state of some benzamide backbone-based oligomers incorporating various alkyl fragments that mimic amino acids, such as leucine, valine, asparagine, lysine, and phenylalanine. We further reasoned that the introduction of the branched alkyl side chain patterns, such as isopropyl, isobutyl, and 2-ethylpentyl, might strengthen the hydrophobic contacts between molecules in the bulk, thus mimicking the binding of small molecules to targeted protein domains. Similar synthetically made backbones have been shown to mimic residues at positions *i*, *i* + 4 and *i* + 7 on the one face of the alpha-helix and successfully disrupt important protein–protein interactions.[8] The design of arylamide scaffolds bearing one or multiple carboxylic acid groups is of particular importance because of their valuable biological properties (*e.g.*, acting as agonists and antagonists of islet amyloid polypeptide (IAPP) aggregation[4,7b,8a] slowing the rate of IAPP assembly associated with type II diabetes pathology). The current work represents a logical extension of earlier efforts on the synthesis and aggregation behavior of benzamide and pyridylamide scaffolds including double alpha-helix mimetics[9] as well as urea-based organogelators[10–12] and benzoylurea mimetics[13] that display similar aggregation properties in the solid state. This manuscript details the morphological characterization of an emerging class of biologically relevant

[a] Department of Chemistry, Massachusetts Institute of Technology, Cambridge, MA, 02139, USA. E-mail: oleg.kulikov.chem@gmail.com, okulikov@mit.edu; Tel: +1 (215) 470-3581

[b] Department of Chemistry, Texas Christian University, Fort Worth, TX, 76129, USA

[c] Department of Chemistry, Indian Institute of Science Education and Research Bhopal, Bhopal 462066, Madhya Pradesh, India

benzamide molecules representing significant interest since activity of therapeutic substances often not only depends on molecular structure, but is also influenced by their morphological form (*i.e.*, higher order supramolecular organization).

Results and discussion

Synthesis

The preparation of the target mono- (**6–9**) and bis-oligoamides **21–28** through the sequential hydrogenation of the nitro group and subsequent amide coupling was previously described[9a] (Scheme 1 and Fig. S1, ESI†):

X-ray studies (single crystal and powder XRD, Chart S1, ESI†)

Inspection of NH$_2$-dimer **6** (Fig. 1, 2 and Fig. S1, ESI†) revealed that molecules are packed in a curved conformation with the side chains projected on different faces in the same manner as that described previously[15] for its structural analogue – dimer **3**. As expected, the curvature of the scaffolds for both compounds (defined as the angle formed by the line drawn from the 1,4-aryl carbons linked to the amide carbonyl to the amide N-linked carbons)
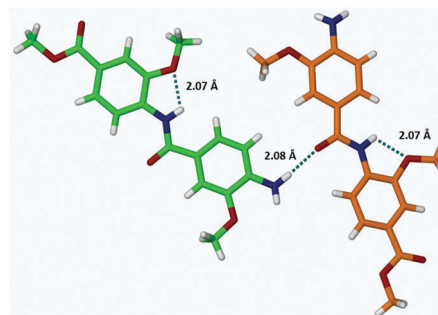

Scheme 1   Structures of mono- and bis-arylamides inspected by electron microscopy.

Fig. 1   Molecular structure of Me-NH$_2$-dimer **6** in comparison with known i-Pr-NH$_2$-dimer (CCDC 851714†) and their overlay (gray for **6** and pink for i-Pr-NH$_2$-dimer) with green arrows indicating rotatable bonds (only polar H atoms are shown).

Fig. 2   Intermolecular H-bonding between NH$_2$- and CO-groups of the neighboring NH$_2$-dimer **6** molecules.
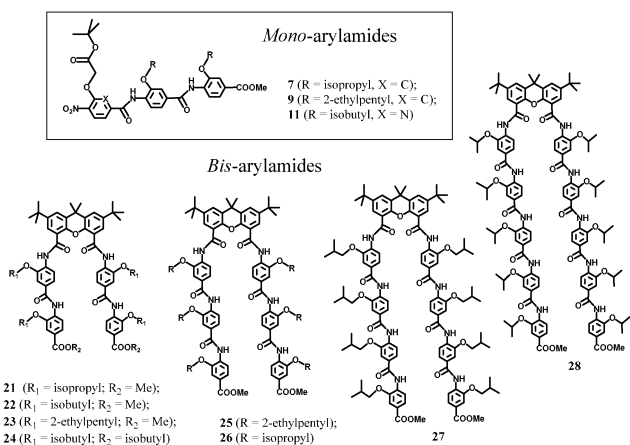
is nearly the same (*i.e.*, 157.6° for NH$_2$-dimer **6** *vs.* 157.7° for **3**, CCDC 851714†). These values are in accordance with the reported data.[14] The intramolecular H-bond between the amide NH and the oxygen of the alkoxy group ($d_{NH\cdots O}$ = 2.07 Å) appears to stabilize the curved oligoamide backbone. A partial crystal packing diagram of **6** showcasing the general H-bonded motif is depicted in Fig. 2 (NH$_2\cdots$O=C, 2.08 Å).

Importantly, in the crystal lattice, molecules of compound **6** tend to pack in a "two-sided" alternating supramolecular pattern as a result of the aforementioned intermolecular H-bonding (NH-groups of the amide fragments are not involved in this interaction, presumably due to the steric hindrance, Fig. S1, ESI†).

According to the single-crystal X-ray analysis, molecules of benzamide dimer **6** are linked together by the NH$_2\cdots$O=C hydrogen bond which was previously reported for its isopropyl, isobutyl, and 2-ethylpentyl analogs.[14,15] Interestingly, this type of supramolecular contact could even be observed for the simplest NH$_2$-monomer **S1**,[16] whereas one of the most complex molecular architectures among the known mono-oligoarylamides was discovered by single-crystal X-ray analysis for pentameric pyridylamide[4] adopting a curved conformation (Fig. S2, ESI†). The molecular geometries of some xanthene-based monomers and the dimeric double alpha-helix mimetics have already been explored.[9a] Most of the structures have been shown to adopt a non-planar conformation as a result of both repulsive inter-actions and crystal-packing forces. Predictably, bis-dimers **21** and **22** showed "out-of-plane" molecular arrangements (Fig. 3 and Fig. S3, S4, ESI†). Thus, compound **21** demonstrated essentially a "puckered" conformation that is likely stabilized by intramolecular H-bonding (*i.e.*, NH$\cdots$O$_{(i-Pr)}$, 2.14–2.23 Å; NH$\cdots$O$_{(xanthene)}$, 2.11–2.12 Å) as well as π–π stacking inter-actions of aromatic rings located on the opposite sides of the bis-arylamide molecule with a centroid-to-centroid distance of 3.61–3.68 Å (Fig. 3, left).

Notably, there are two crystallographically independent molecules of compound **21** in the asymmetric unit, and in addition to that, two molecules of ethanol and one of water (ESI,† Fig. S3).

While molecules of i-Pr-bis-dimer **21** are involved in H-bonding interactions with water and EtOH, no solvent matrix associated with i-Bu-bis-dimer **22** was found in its crystal
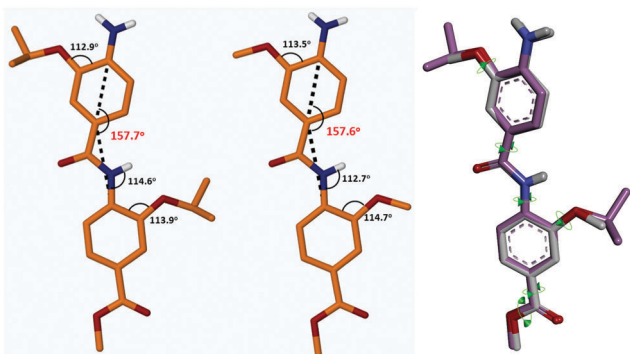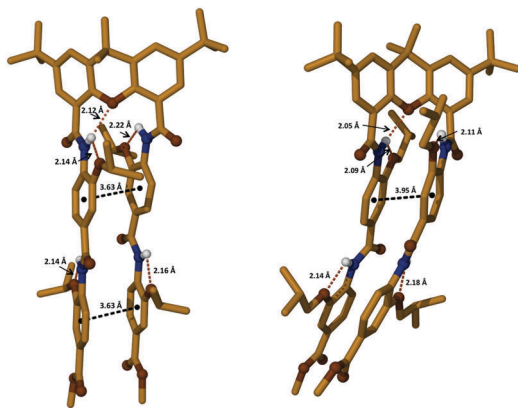
Fig. 3 Molecular structures of i-Pr-bis-dimer **21** (left) and i-Bu-bis-dimer **22** (right). Only one of two crystallographically unique molecules of dimer **21** is shown.

lattice. Unlike bis-dimer **21**, molecules of compound **22** bearing isobutyl side chains showed appreciably greater curvature of both arylamide rods. Otherwise unremarkable changes in the molecular geometry were observed except for the xanthene moiety that is almost planar in the case of **22** (the dihedral angle between the aromatic rings is 160.8° *vs.* 136.2° (134.0°) found for **21**, Fig. S5, ESI†). We attribute these differences to the crystal packing forces. As expected, intramolecular hydrogen bonding values for compound **22** fall in the 2.09–2.18 Å range for NH···O$_{(i-Bu)}$ contacts and are found to be of 2.05 Å for NH···O$_{(xanthene)}$ interactions. Clearly, π–π stacking plays a very important role in arranging i-Pr-bis-dimer **21** molecules into supramolecular arrays (Fig. 4); however, in certain cases the intermolecular distances between aromatic rings are longer than those currently accepted.[17] Also, we presume that the (NH–CO) dipole stacking[18a,b] of the adjacent molecules may contribute appreciably to the supramolecular organization of bis-oligoamides in the crystal lattice (Fig. S5-2, 3, 4, 5, ESI†) and even compete with H-bonding; however, the direct experimental determination of the dipole moments[18c–f] of the individual

amide bonds and their correlation with bis-arylamide structure as a whole seems to be a quite complicated matter. In addition to this, molecules of **21** belonging to the different layers were found to interlock using their *tert*-butyl groups attached to the xanthene moiety (Fig. S6–S9, ESI†).

Similarly, molecules of i-Bu-bis-dimer **22** appear to self-assemble into supramolecular chains as a result of extensive "face-to-face" π–π stacking interactions (d = 3.59 Å, Fig. 5). More complex supramolecular arrangements could be found in the ESI† (Fig. S10 and S11). Previously reported[9a] bis-dimer **23** with branched 2-ethylpentyl side chains exhibited a similar "stacked" packing motif.

The XRD pattern recorded for a powder sample of i-Bu-bis-dimer **22** (Fig. 6) is indicative of the high crystallinity of this compound, which is in agreement with the above-mentioned single-crystal X-ray data. Multiple sharp peaks can be attributed to the interlayer distances in crystal packing. Thus, higher order reflection peaks at 2θ = 19.20° and 24.97° (d = 4.6 and 3.6 Å, correspondingly) may refer to stacking interactions with the distances matching up closely with the aromatic centroid/centroid separations illustrated in Fig. 5. The other peaks observed in these patterns could also arise from the self-assembly properties of **22**. Remarkably, the XRD profile of bis-pentamer **28** (Fig. S12, ESI†) demonstrated a strong first-order peak at 2θ = 9.15° (d = 9.7 Å) and plenty of broad overlapping peaks in the 2θ range of 15–26°. This is not unexpected since the extended oligomer rods would likely offer more conformational freedom.

Microscopic examination of the mono- and bis-oligoamides using electron microscopy techniques (TEM, SEI, and SEM), Chart S2, ESI†

In order to investigate the behavior of the representative mono- and bis-oligoamide scaffolds at the micron and submicron levels, we have employed transmission electron microscopy (TEM), secondary electron imaging (SEI), and scanning electron microscopy (SEM). Thus, the images shown in panels a–d of Fig. 7 demonstrate the range of microfibers observed. Although
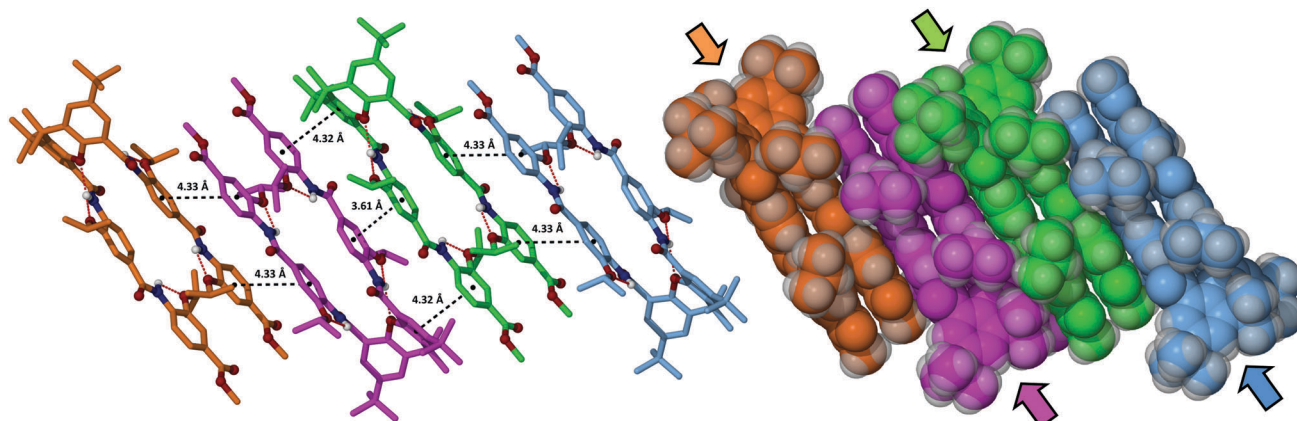

Fig. 4 Partial packing diagram of i-Pr-bis-dimer **21** (stick and CPK formats): selected centroid (Ar)···centroid (Ar) distances between the adjacent molecules. Non-polar hydrogen atoms are omitted for clarity (arrows in the left structure indicate the relative orientation of bis-dimer molecules with respect to each other).
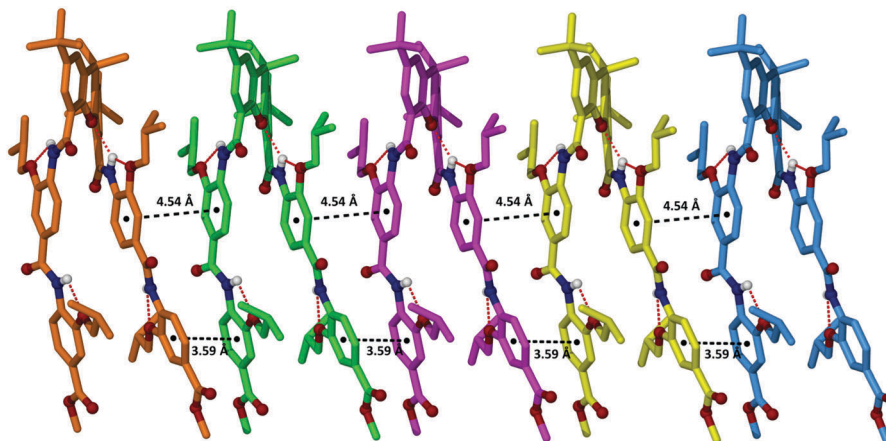
Fig. 5 Partial packing diagram of i-Bu-bis-dimer **22**: selected centroid (Ar)···centroid (Ar) distances between the adjacent molecules. Non-polar hydrogen atoms are omitted for clarity.
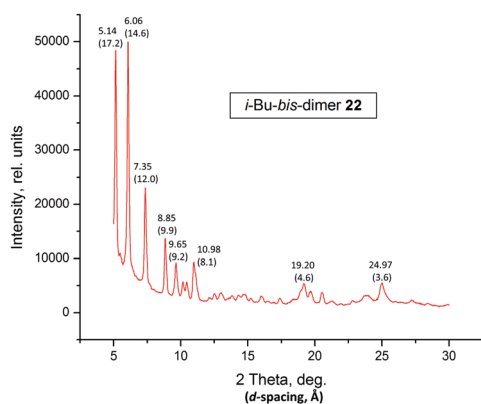

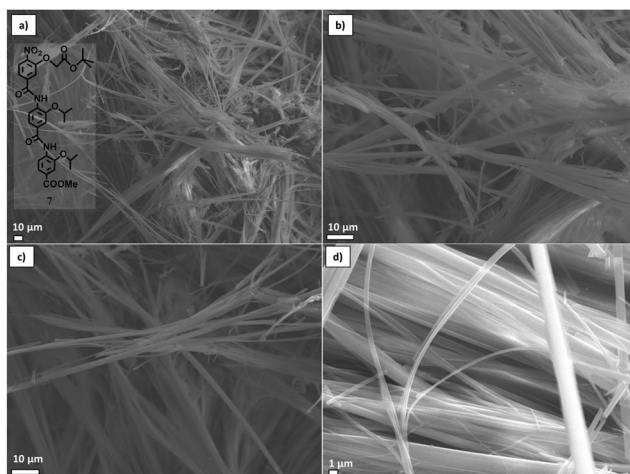**Fig. 6** Powder XRD patterns of i-Bu-bis-dimer **22**.

Fig. 7 SEI of fibrillar aggregates formed from trimer **7** (panels a–d). Scale bar: 10 μm (panels a–c, e–h) and 1.0 μm (panel d), with a 1 : 1 (v/v) mixture of EtOAc/CHCl₃.

most of the aggregates depicted in Fig. 7 (panels a–c) have a diameter of ∼1–5 μm, the presence of fibers with a thickness under 1 μm and a total length of ∼30–60 μm (Fig. 7d) is apparent.

This might be due to extensive intermolecular hydrogen bonding between trimer molecules as well as hydrophobic side chain interactions leading to the formation of supramolecular arrangements that resemble the patterns depicted in Fig. 2 and Fig. S1 (ESI,† vol. 1). In general, the morphology assembled from the other trimers **9** and **11** showed structural similarities to the aggregation behaviors of **7** in the solid state, and insignificant differences in appearance might account for the variation of the side chains (*i.e.*, isopropyl, **7**; 2-ethylpentyl, **9**; isobutyl, **11**; Fig. 2S1, 2S2 and 2S3; ESI,† vol. 2). Overall, the SEI findings for the arylamide trimers are suggestive of a general trend to form fiber-like crystals under a variety of conditions employed. Further studies of bis-oligoamides having two arylamide rods provided valuable insight into the aggregation modes of this type of molecule, in particular, how the number of repeat units in the oligomer structure may define specific secondary motifs.

Thus, we have shown that bis-trimer **26** is prone to organize into microfibers upon slow evaporation of the corresponding stock solutions (Fig. 2S4; ESI,† vol. 2) with the thickness of the aggregates varying from 1 to 10 μm. In order to examine the aggregation behavior of bis-oligoamides as a function of concentration, we have prepared and inspected (by both TEM and SEM techniques) a series of DMF stock solutions (*i.e.*, bis-tetramer **27** bearing isobutyl side chains; $C = 10$ mg mL^{-1} (panel a), 5 mg mL^{-1} (panel b), 2.5 mg mL^{-1} (panel c), 1.25 mg mL^{-1} (panel d), 0.625 mg mL^{-1} (panel e), and 0.313 mg mL^{-1} (panel f), Fig. 8). Interestingly, successive dilution of bis-tetramer **27** afforded both concentration-dependent fibrous aggregates and spherical particles clearly visible in panels e and f.

The SEM findings for bis-tetramer **27** (Fig. 9, panels a–f) deposited from DMF stock solutions generally are in agreement with the trend mentioned above (*i.e.*, extensive aggregation of fibers at high concentration and the presence of small spheres when the specimen was prepared from diluted stocks).

In contrast to the aggregation properties of bis-tetramer **27** in DMF, its structural homologues **21** (Fig. 2S5; ESI,† vol. 2) and **22** having a shorter benzamide scaffold tend to produce arrays of microspheres as evident by both TEM and SEM studies.
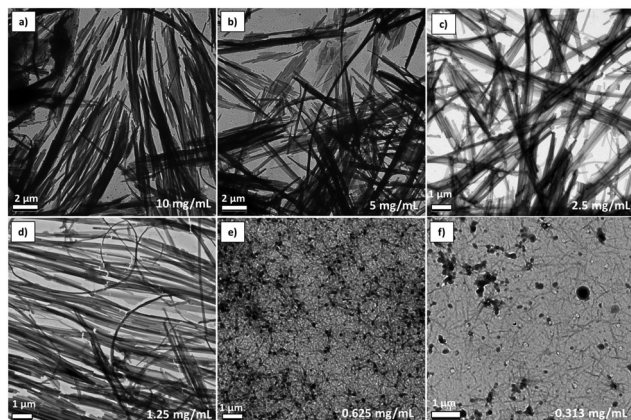
Fig. 8 TEM micrographs of bis-tetramer **27**: the formation of a micro-fibrillar network (panels a–f) at different concentrations. Scale bars: 2 μm (panels a and b); 1 μm (panels c–f).
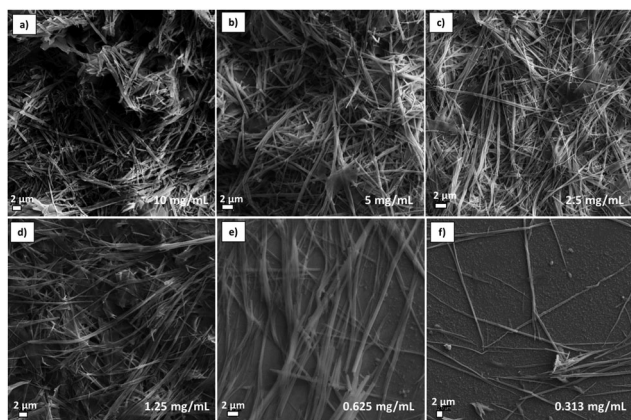

Fig. 9 SEM micrographs of bis-tetramer **27**: the formation of microfibers (panels a–f) at different concentrations. Scale bars: 2 μm (panels a–f).
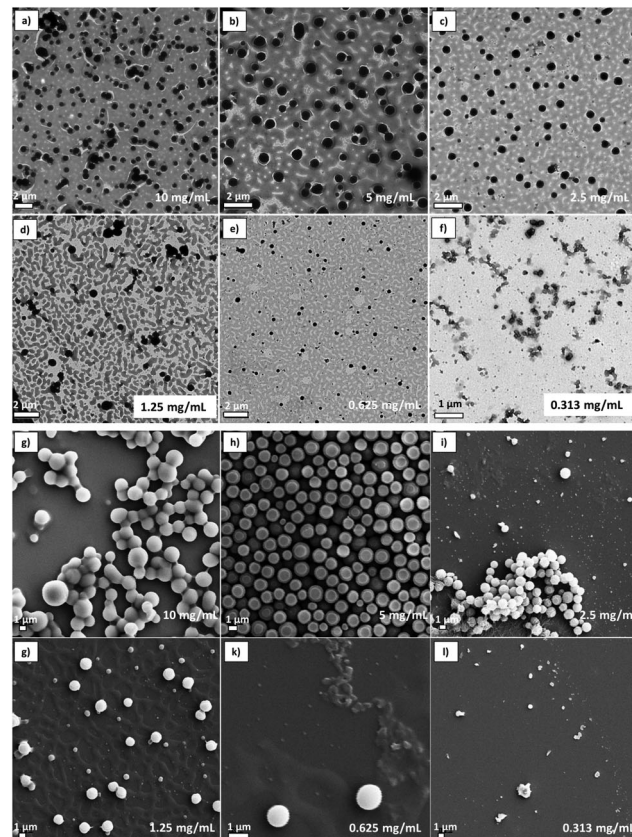

Fig. 10 TEM (a–f) and SEM (g–l) micrographs of bis-dimer **22**: spherical aggregates at different concentrations. Scale bars: 2 μm (panels a–e); 1 μm (panels f–l).

Thus, panels of Fig. 10 illustrate a variety of spherical nano-particles self-assembling from bis-dimer **22** when deposited from DMF stock solutions on the Si-substrate at concentrations ranging from 10 to 0.313 mg mL^{-1}. It is remarkable to observe dramatic changes in the appearance of aggregates in comparison to the previously shown dimer **27**.

Notably, for both bis-dimer **22** and its respective bis-tetramer **27**, their morphology type persists at least within the range of concentrations explored.

To understand the effect of varying the alkyl side chains in bis-dimers on the type of aggregated morphology, we have examined compounds **23** and **24** having the same benzamide backbone as that of bis-dimer **22**. The findings for these two compounds generally complement the observations for bis-dimer **22**, *i.e.*, a tendency to form spheres upon deposition from DMF stocks. More images of bis-dimers **22** and **23** emphasizing the formation of spherical aggregates can be found in the ESI,† vol. 2 (Fig. 2S6, 2S7 and 2S8, ESI†). Very distinct spherical particles (with a diameter of 2 μm and less) identified by SEM for bis-dimer **24** are believed to assemble upon slow solvent evaporation (Fig. 11a–d and Fig. 2S9, 2S10, 2S11; ESI,† vol. 2). In general, deposition of all bis-dimers

from DMF stocks is favorable to the formation of microspheres. It appeared that the solvent change for bis-dimer **24** (*i.e.*, DMF to EtOAc/CHCl₃) yielded fibrillar aggregates (Fig. 2S12 and 2S13). We hypothesize that the presence of two additional isobutyl groups in the structure of **24** (if compared with its homologue **22**) facilitates hydrophobic side chain interactions.

Thus, it is worth mentioning that the elongation of benzamide scaffolds for higher oligoamides (that was exemplified by comparison of the bis-dimer structure with its respective bis-tetramer) displayed an adverse effect on the morphologies identified both by TEM and SEM techniques. This can be attributed to the ability of higher oligomer molecules to fuse together providing bundled supramolecular architectures that appeared as fibrous aggregates when visualized by electron microscopy. More representative images (*e.g.*, bis-trimer **25**, bis-tetramer **27**, and bis-pentamer **28**) that support the hypothesis of the predominant formation of fibers/rod-like motifs for the higher oligomers are reported in the ESI,† vol. 2 (Fig. 2S14, 2S14-2 and 2S14-3, correspondingly).

Furthermore, we realize that the specific morphological motif may result from the interplay of molecular structures, solvents of choice, deposition temperatures, substrates, *etc.*

Polarized optical microscopy (POM) studies

POM determination of a series of small mono-, bis- and tris-urea molecules possessing interesting liquid crystalline properties
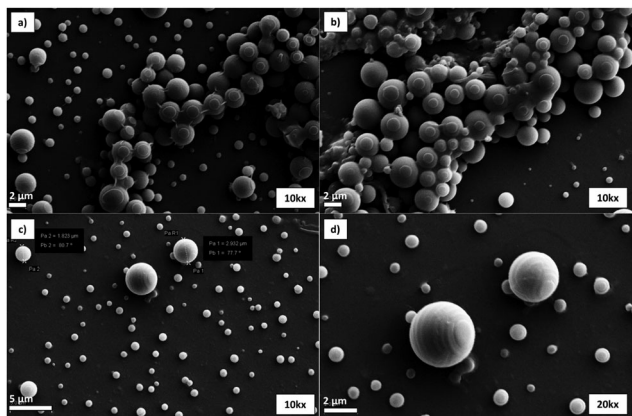
Fig. 11 SEM images of bis-dimer **24** deposited from DMF (panels a–d). Scale bars: 2 μm (panels a, b and d); 5 μm (panel c).
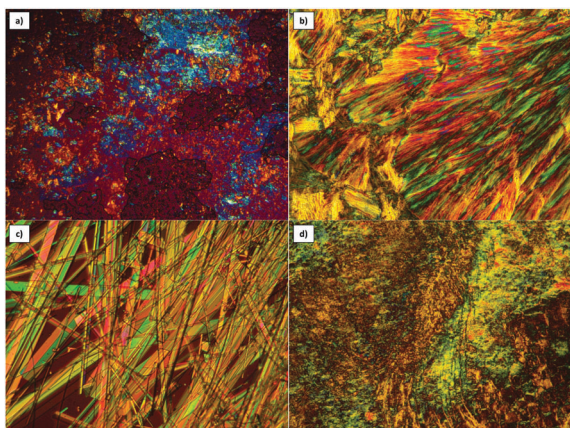

Fig. 12 POM micrographs (10×) of bis-tetramer **27** (panel a), bis-dimer **22** (panel b), bis-dimer **23** (panel c), and bis-pentamer **28** (panel d) deposited from DMF stocks.

has been previously reported.[12] In the current work, polarized optical microscopy images have been obtained from exemplary bis-oligoamides **22–25**, **27**, and **28** (Fig. 12 and Fig. 2S15, 2S16, 2S17, 2S18, 2S19; ESI,† vol. 2) to provide evidence for self-assembly. Seemingly, birefringent textures, fibers, and rod-like aggregates/crystals appeared under polarized light are indicative of the small molecule self-assembly that was discussed above.

We hypothesize that the very bright colorful texture seen in panel b of Fig. 12 stands for the smectic phase implying the positional and directional order for bis-dimer **22** molecules. Higher bis-oligoamides (*i.e.*, bis-tetramer **27** and bis-pentamer **28**; panels a and d of Fig. 12) showed similar morphologies.

Conclusions

The current work is mostly focused on the self-assembly properties of mono- and bis-oligoamides, potential α-helix mimetics, studied by a combination of single-crystal X-ray diffraction analysis, powder XRD, electron microscopy (*i.e.*, SEI, SEM, TEM techniques), and polarized optical microscopy (POM).

To clarify the morphology/structure dependence, dilution experiments were carried out on bis-tetramer **27** and its parent dimer structure **22**. Two concentration series performed on bis-oligoamides bearing the same isobutyl side chain in DMF revealed the predominant formation of micro- and nanofibers for the bis-tetramer as well as spherical aggregates for its respective bis-dimer analogue. To generalize the bis-dimer **22** results, we investigated two additional dimeric scaffolds (compounds **23** and **24**) having different peripheral substituents, which exhibited a similar trend to assemble into spheres. Thus, the TEM analysis of the DMF dilution series closely matching the SEM data for compounds **22** and **27** suggests that aggregation is likely influenced by the number of repeat units in the oligomer structure (*i.e.*, longer oligomer scaffolds favor the formation of fibrillar aggregates). To prove this hypothesis, we inspected other higher oligomers, such as bis-trimer **25** and bis-pentamer **28**, which similarly displayed fibers upon deposition from DMF. Another important practical aspect of this work is that morphological behaviors are solvent dependent (*e.g.*, bis-dimer **24** deposition from DMF or EtOAc/CHCl$_3$ leads to vastly different motifs) which may be used for the fine-tuning of the material properties.

In a more general sense, these aggregation behaviors may arise from self-association driven by the cooperative interplay of non-covalent interactions including H-bonding, hydrophobic side chain interactions, and π–π stacking as shown previously for urea molecules,[12,19,20] and that is generally related to the supramolecular recognition process.[21] Additionally, there may be amide dipole stacking of oligoamides in the solid state. The remarkable liquid crystalline properties of these compounds are indicative of molecular self-assembly. The aforementioned highly specific morphological properties will require very careful investigation and consideration since α-helix mimetics' strong aggregation may affect protein binding and drug efficiency. Overall, these extensive structural studies provide insight into the experimental methodology (*e.g.*, tuning secondary structures), which can be successfully exploited to design complex supramolecular systems from biologically relevant molecules through directed self-assembly.

Acknowledgements

References

1 (*a*) *Foldamers: Structure, Properties and Applications*, ed. S. Hecht and I. Huc, Wiley-VCH, Weinheim, 2007; (*b*) J. Iriondo-Alberdi, K. Laxmi-Reddy, B. Bouguerne, C. Staedel and I. Huc, *ChemBioChem*, 2010, **11**, 1679–1685; (*c*) B. Baptiste, C. Douat-Casassus, K. Laxmi-Reddy, F. Godde and I. Huc, *J. Org. Chem.*, 2010, **75**, 7175–7185; (*d*) X. Zhao

and Zh.-T. Li, *Chem. Commun.*, 2010, **46**, 1601–1616; (*e*) G. M. Burslem, H. F. Kyle, P. Prabhakaran, A. L. Breeze, T. A. Edwards, S. L. Warriner, A. Nelson and A. J. Wilson, *Org. Biomol. Chem.*, 2016, **14**, 3782–3786; (*f*) L. Sebaoun, B. Kauffmann, T. Delclos, V. Maurizot and I. Huc, *Org. Lett.*, 2014, **16**, 2326–2329.

2 (*a*) C. G. Cummings and A. D. Hamilton, *Curr. Opin. Chem. Biol.*, 2010, **14**, 341–346; (*b*) P. Restorp and J. Rebek, Jr., *Bioorg. Med. Chem. Lett.*, 2008, 5909–5911; (*c*) J. P. Plante, T. Burnley, B. Malkova, M. E. Webb, S. L. Warriner, T. A. Edwards and A. J. Wilson, *Chem. Commun.*, 2009, 5091–5093; (*d*) L. Moisan, S. Odermatt, N. Gombosuren, A. Carella and J. Rebek, *Eur. J. Org. Chem.*, 2008, 1673–1676; (*e*) S. Marimganti, M. N. Cheemala and J.-M. Ahn, *Org. Lett.*, 2009, **11**, 4418–4421; (*f*) P. Tosovska and P. S. Arora, *Org. Lett.*, 2010, **12**, 1588–1591; (*g*) V. Haridas, *Eur. J. Org. Chem.*, 2009, 5112–5128; (*h*) A. J. Wilson, *Chem. Soc. Rev.*, 2009, **38**, 3289–3300; (*i*) A. Shaginian, L. R. Whitby, S. Hong, I. Hwang, B. Farooqi, M. Searcey, J. Chen, P. K. Vogt and D. L. Boger, *J. Am. Chem. Soc.*, 2009, **131**, 5564–5572; (*j*) J. H. Lee, Q. Zhang, S. Jo, S. C. Chai, M. Oh, W. Im, H. Lu and H.-S. Lim, *J. Am. Chem. Soc.*, 2011, **133**, 676–679; (*k*) V. Azzarito, J. A. Miles, J. Fisher, T. A. Edwards, S. L. Warriner and A. J. Wilson, *Chem. Sci.*, 2015, **6**, 2434–2443; (*l*) S. Rodriguez-Marin, N. S. Murphy, H. J. Shepherd and A. J. Wilson, *RSC Adv.*, 2015, **5**, 104187–104192; (*m*) P. Ravindranathan, T.-K. Lee, L. Yang, M. M. Centenera, L. Butler, W. D. Tilley, J.-T. Hsieh, J.-M. Ahn and G. V Raj, *Nat. Commun.*, 2013, **4**, 1923.

3 I. Saraogi, C. D. Incarvito and A. D. Hamilton, *Angew. Chem., Int. Ed.*, 2008, **47**, 9691–9694.

4 I. Saraogi, J. A. Hebda, J. Becerril, L. A. Estroff, A. D. Miranker and A. D. Hamilton, *Angew. Chem., Int. Ed.*, 2010, **49**, 736–739.

5 S. Fletcher and A. D. Hamilton, *Curr. Opin. Chem. Biol.*, 2005, **9**, 632–638.

6 (*a*) I. Saraogi and A. D. Hamilton, *Biochem. Soc. Trans.*, 2008, **36**, 1414–1417; (*b*) M. K. P. Jayatunga, S. Thompson and A. D. Hamilton, *Bioorg. Med. Chem. Lett.*, 2014, **24**, 717–724; (*c*) C. G. Cummings and A. D. Hamilton, *Tetrahedron*, 2013, **69**, 1663–1668.

7 (*a*) I. Saraogi and A. D. Hamilton, *Chem. Soc. Rev.*, 2009, **38**, 1726–1743; (*b*) O. V. Kulikov, S. Kumar, M. Magzoub, P. C. Knipe, S. Thompson, A. D. Miranker and A. D. Hamilton, *Tetrahedron Lett.*, 2015, **56**, 3670–3673; (*c*) J. Seidler, S. L. McGovern, T. N. Doman and B. K. Shoichet, *J. Med. Chem.*, 2003, **46**, 4477–4486; (*d*) B. Y. Feng and B. K. Shoichet, *Nat. Protoc.*, 2006, **1**, 550–553.

8 (*a*) S. Kumar, D. E. Schlamadinger, M. A. Brown, J. M. Dunn, B. Mercado, J. A. Hebda, I. Saraogi, E. Rhoades, A. D.

Hamilton and A. D. Miranker, *Chem. Biol.*, 2015, **22**, 369–378; (*b*) W. E. Martucci, J. M. Rodriguez, M. A. Vargo, M. Marr, A. D. Hamilton and K. S. Anderson, *MedChemComm*, 2013, **4**, 1247–1256.

9 (*a*) O. V. Kulikov, S. Thompson, H. Xu, C. D. Incarvito, R. T. W. Scott, I. Saraogi, L. Nevola and A. D. Hamilton, *Eur. J. Org. Chem.*, 2013, 3433–3445; (*b*) L. Nevola, J. M. Rodriguez, S. Thompson and A. D. Hamilton, *Supramol. Chem.*, 2013, **25**, 586–590.

10 G. Wang and A. D. Hamilton, *Chem. – Eur. J.*, 2002, **8**, 1954–1961.

11 G. Wang and A. D. Hamilton, *Chem. Commun.*, 2003, 310–311.

12 O. V. Kulikov, D. A. Siriwardane, G. T. McCandless, C. Barnes, Y. V. Sevryugina, J. D. DeSousa, J. Wu, R. Sommer and B. M. Novak, *Eur. J. Org. Chem.*, 2015, 7511–7518.

13 S. Thompson and A. D. Hamilton, *Org. Biomol. Chem.*, 2012, **10**, 5780–5782.

14 O. V. Kulikov, C. Incarvito and A. D. Hamilton, *Tetrahedron Lett.*, 2011, **52**, 3705–3709.

15 O. V. Kulikov and A. D. Hamilton, *RSC Adv.*, 2012, **2**, 2454–2461.

16 L. A. Estroff, C. D. Incarvito and A. D. Hamilton, 5-Amino-6-*tert*-butoxycarbonylmethoxypyridine-2-carboxylic acid methyl ester (S1) was synthesized according to a literature procedure, *J. Am. Chem. Soc.*, 2004, **126**, 2–3. Partial crystal packing diagram (Fig. S2, ESI†) clearly demonstrated intermolecular hydrogen bonding resulted in formation of supramolecular chains.

17 M. Nishio, *CrystEngComm*, 2004, **6**, 130–158.

18 (*a*) W. H. James III, C. W. Muller, E. G. Buchanan, M. G. D. Nix, L. Guo, L. Roskop, M. S. Gordon, L. V. Slipchenko, S. H. Gellman and T. S. Zwier, *J. Am. Chem. Soc.*, 2009, **131**, 14243–14245; (*b*) W. H. Pirkle, *Tetrahedron Lett.*, 1983, **24**, 5707–5708; (*c*) W. D. Kumler and C. W. Porter, *J. Am. Chem. Soc.*, 1934, **56**, 2549–2554; (*d*) O. Exner and Z. Papouskova, *Collect. Czech. Chem. Commun.*, 1980, **45**, 2410–2416; (*e*) M. M. Rodrigo, M. P. Tarazona and E. Saiz, *J. Phys. Chem.*, 1986, **90**, 5565–5567; (*f*) W. W. Bates and M. E. Hobbs, *J. Am. Chem. Soc.*, 1951, **73**, 2151–2156.

19 F. Piana, D. H. Case, S. M. Pamalhete, G. Pileio, M. Facciotti, G. M. Day, Y. Z. Khimyak, J. Angulo, R. C. D. Brown and P. A. Gale, *Soft Matter*, 2016, **12**, 4034–4043.

20 N. Busschaert, C. Caltagirone, W. V. Rossom and P. A. Gale, *Chem. Rev.*, 2015, **115**, 8038–8155.

21 (*a*) K. Fujita, S. Fujiwara, T. Yamada, Yu. Tsuchido, T. Hashimoto and T. Hayashita, *J. Org. Chem.*, 2017, **82**, 976–981; (*b*) A. J. Goshe, I. M. Steele, C. Ceccarelli, A. L. Rheingold and B. Bosnich, *Proc. Natl. Acad. Sci. U. S. A.*, 2002, **99**, 4823–4829.